

ARTICLE

Untangling surface oxygen exchange effects in $\text{YBa}_2\text{Cu}_3\text{O}_{6+x}$ thin films by electrical conductivity relaxation

P. Cayado^a, C. F. Sánchez-Valdés^a, A. Stangl^a, M. Coll^a, P. Roura^b, A. Palau^a, T. Puig^a and Xavier Obradors^{a,*}

Received 00th January 20xx,
Accepted 00th January 20xx

DOI: 10.1039/x0xx00000x

www.rsc.org/

The kinetics of oxygen in-corporation (in-diffusion process) and ex-corporation (out-diffusion process), in $\text{YBa}_2\text{Cu}_3\text{O}_{6+x}$ (YBCO) epitaxial thin films prepared using the Chemical Solution Deposition (CSD) methodology by the Trifluoroacetate route, was investigated by electrical conductivity relaxation measurements. We show that oxygenation kinetics of YBCO films is limited by the surface exchange process of oxygen molecules prior to bulk diffusion into the film. The analysis of temperature and oxygen partial pressure influence on the oxygenation kinetics has drawn a consistent picture of the oxygen surface exchange process enabling us to define the most likely rate determining step. We have also established a strategy to accelerate the oxygenation kinetics at low temperatures based on the catalytic influence of Ag coatings thus allowing to decrease the oxygenation temperature in the YBCO thin films.

Introduction

The use of low-cost techniques such as Chemical Solution Deposition (CSD) for the growth of high performance $\text{REBa}_2\text{Cu}_3\text{O}_{6+x}$ (REBCO) Coated Conductors (CCs) is one of the major requirements in obtaining a widespread use of superconductivity in large scale applications^{1–6}. CSD has become a very competitive, cost-effective and scalable methodology to produce REBCO, especially YBCO, epitaxial thin films and so extensive analysis of all the relevant processing steps is worthwhile.

The last step in any CC manufacturing process is oxygenation. Achieving optimal oxygen content in YBCO films is actually a critical issue in the development of high critical current superconductors. This process depends on the kinetics of the surface oxygen exchange and bulk oxygen diffusion processes. Therefore, an improved understanding of oxygen incorporation (in-diffusion process) and ex-corporation (out-diffusion process) in YBCO films is needed to design an optimal oxygenation.

The oxygen exchange processes have been investigated extensively in the past using different techniques such as secondary ion mass spectrometry^{7–9}, thermogravimetry^{10,11}, spectroscopic ellipsometry¹² or electrical conductivity relaxation^{13–19}. However, in most of the cases the kinetics of the oxygen exchange have been analyzed in terms of a volume diffusion process governed by Fick's laws^{20,21} and the surface reactions that the oxygen molecules experience on the YBCO films have been scarcely considered¹⁷.

However, in recent years, the mechanisms of oxygen exchange and bulk diffusion in functional oxides have become a topic generating high interest. The relevance of surface reactions, which may become the slowest step in the whole chain of oxygen exchange, has been stressed. This is particularly important in thin films, because the short diffusion distance makes bulk diffusion very fast

leading to homogeneously oxygenated films. Especially relevant is the research about this issue in the field of solid oxide fuel cells (SOFC) where mixed ionic and electronic conductors (MIEC) are used^{22–24}. In these materials, the oxygen molecules have to complete four different steps before diffusing through the volume: i) adsorption/ionization, ii) surface diffusion to find a vacancy, iii) dissociation and iv) migration of the second ion to find another vacancy^{25–27}.

Among these steps, the slowest one limits the overall rate of the surface reaction and, for this reason, it is known as rate determining step (rds). The rds can vary depending on the particular case that is being considered. Similar proposals have been made for many MIECs, such as SrTiO_3 (STO), Fe-Doped STO or $\text{Ba}_{1-x}\text{Sr}_x\text{Co}_y\text{Fe}_{1-y}\text{O}_{3-z}$ ^{28–32}. Also, extensive analysis of the oxygen surface reactions have been carried out in CeO_{2-z} (ceria) and gadolinium doped ceria (GDC), as recognized oxygen-deficient compounds which may serve as model systems. The complexity of the surface oxygen-ion transfer was demonstrated on these systems and it was shown that surface phenomena can limit in some cases the rate of the overall oxygen exchange processes^{33–39}. However, the possibility that the surface reactions limited the oxygen exchange processes in YBCO films was mostly discarded and only recently it was pointed out the role of surface reactions^{12,17,40}. Therefore, further analysis of the oxygen exchange mechanisms in YBCO films is needed to sort out when this process is surface limited and under which conditions the volume bulk diffusion in films is indeed fast enough.

For this reason, in this work, we analyze, by electrical conductance relaxation measurements, the effect that several parameters, such as temperature (T) and oxygen partial pressure (PO_2), have on the oxygenation kinetics of CSD YBCO films. After concluding that surface exchange effects play the key role in oxygenating our YBCO films we also investigate the influence of including Ag as catalyst to enhance the low temperature oxygenation rate. The results are the base for designing optimal oxygenation processes in minimal time for YBCO films having different oxygen contents.

^a Institut de Ciència de Materials de Barcelona (CSIC), Campus UAB, 08193, Bellaterra, Catalonia, Spain

^b University of Girona, Montilivi Campus, Edif. PII, E17071, Girona, Catalonia, Spain

Theoretical aspects

The problem of oxygen diffusion in YBCO thin films is addressed, in a simple way, as a one-dimensional diffusion process in a homogeneous medium bounded by two parallel infinite planes, e.g. the planes at $x=0$ and $x=l$ (actually, we only have one limiting surface because the other one is in contact with the substrate). These conditions apply in practice to diffusion into a plane sheet of material so thin that effectively all the diffusing substance enters through the plane faces and a negligible amount through the edges. In this case the problem is reduced to solve the second Fick's law in one dimension (Equation 1)^{20,21,41}:

$$\frac{\partial C}{\partial t} = D \left(\frac{\partial^2 C}{\partial x^2} \right) \quad (\text{Equation 1})$$

with boundary conditions of zero flux at the film-substrate interface,

$$\left. \frac{\partial C}{\partial x} \right|_{x=0} = 0$$

and a linear reaction rate at the free surface,

$$D \left. \frac{\partial C}{\partial x} \right|_{x=l} = k_S (C_{eq} - C_S)$$

where D is the mean value of the bulk diffusion coefficient in the material, k_S is the surface reaction rate constant, l is the film thickness and C , C_S and C_{eq} are its oxygen concentration at any point, at the surface and that in equilibrium with the surrounding gas, respectively.

For an initial homogeneous oxygen concentration, C_0 , this problem has an exact analytical solution⁴¹. This solution integrated over the film thickness delivers the time-dependence of the average oxygen concentration, \bar{C} (Equation 2):

$$\frac{\bar{C} - C_0}{C_{eq} - C_0} = 1 - \sum_{n=1}^{\infty} A_n e^{-t/\tau_n} \quad (\text{Equation 2})$$

where

$$\tau_n \equiv l^2 / (\beta_n^2 D); \quad A_n \equiv \frac{2\delta^2}{\beta_n^2 (\beta_n^2 \delta^2 + \delta)} \quad \text{and} \quad \delta \equiv lk_S / D.$$

The values β_n are the n 'th positive roots of (Equation 3):

$$\beta_n \tan \beta_n = \delta \quad (\text{Equation 3})$$

For a volume diffusion-controlled process ($\delta \gg 1$) and for a surface-controlled process ($\delta \ll 1$), the only relevant term of the series of the solution is the first one; the other terms have much shorter time constants and much lower amplitudes. Consequently, in both cases the evolution with time of \bar{C} can be described by a single time constant (Equation 4):

$$\frac{\bar{C} - C_0}{C_{eq} - C_0} \approx 1 - e^{-t/\tau} \quad (\text{Equation 4})$$

where $\tau = \frac{l^2}{2\pi^2 D}$ or $\tau = 1/k_S$ is the relaxation time if the process is volume-diffusion or surface exchange-controlled, respectively.

In the case that the process was volume-diffusion controlled, the exponential function should be multiplied by a factor very close to one ($8/\pi^2$).

Finally, since oxygen content controls the electronic carrier concentration in YBCO films, its evolution will result in a parallel evolution of the film conductance, $G=1/R$. We will assume that \bar{C} and G are proportional (i.e., the mobility of the carriers are assumed to be constant during the course of relaxation) and, consequently, the electrical conductance transients will be fitted to the time dependence of equation 5, where concentrations must be substituted by the conductances (Equation 5):

$$\frac{G(t) - G_0}{G_{\infty} - G_0} \propto 1 - e^{-\left(\frac{t}{\tau}\right)} \quad (\text{Equation 5})$$

Eventually, if there are two different parallel oxygenation channels it would be necessary to consider two conductivity relaxation processes with different relaxation times¹⁷.

Results

Structural characterization of the films

All the 250 nm CSD YBCO films employed in this study present excellent biaxial texture as it is observed in the 2D XRD θ - 2θ frame (Figure 1a)) and confirmed by ϕ -scan measurements and ω -scan measurements (typically $\Delta\omega \sim 0.6^\circ$). The YBCO grains exhibit a perfect epitaxial (001) orientation (Figure 1b)). Presence of other grain orientation or secondary phases is not detected.

On the other hand, the SEM image shown in figure 2 demonstrates that the obtained films have a dense and homogenous surface without presence of precipitates or grains with {100} planes oriented perpendicular to the substrate (a-b grains). It is remarkable the presence of pores (marked with white arrows) that have a great importance in the oxygen diffusion processes, as it will be discussed later.

Temperature dependence of oxygenation kinetics

The electrical conductivity relaxation after consecutive steps of PO_2 , either going towards a lower value ($P_L = 2 \times 10^{-4}$ atm) or towards a higher value ($P_H = 1$ atm), can be observed in figure 3a). The consecutive conductance steps are measured at different temperatures.

When PO_2 decreases, oxygen ions leave the YBCO structure (we will refer to this process as "out-diffusion"), thus decreasing the carrier concentration and so causing a decrease of the film conductance (Figure 3b). This process leads to a final stoichiometry close to $YBa_2Cu_3O_6$ and, therefore, a change from the orthorhombic phase to the tetragonal phase obtaining a non-superconducting film. The oxygen level can be estimated from the T- PO_2 phase diagram⁴²⁻⁴⁴. On the other hand, when PO_2 increases, oxygen ions go into YBCO (process referred as "in-diffusion") and an increase of the conductance is observed (Figure 3c)). During the in-diffusion processes we come back to the orthorhombic phase and the films become superconducting again. The different values of oxygen stoichiometry can be again estimated accordingly to the T and the PO_2 and this will determine the T_c of the films⁴⁵. Notice that the saturation values of the conductance at P_L and at P_H increase when temperature is lower. This evolution is mainly due to the increase of the equilibrium oxygen content at low temperatures and higher PO_2 values^{42,46}. The saturation conductance is shown to decrease at high temperatures, independently of the metallic to semiconducting transition of the YBCO films at an oxygen content $\delta \sim 0.6$. This would indicate that the influence of the carrier concentration change in the conductance overcomes the intrinsic temperature dependence of the electric conductivity of the YBCO phase in the semiconductor

or metallic regimes. Figures 3a) and 3b) also show that at low temperatures (below 550 °C for the out-diffusion and below 400 °C for the in-diffusion) the saturation of the conductance is not reached. This is because, at such low temperatures, the oxygen exchange process is so slow that the equilibrium is not reached at lab scale times (maximum 2h in the present experiments). Figure 3b) shows one example of not saturated out-diffusion process measured at 400 °C, even if much longer annealing times are used (> 15 h).

as discussed in section 3. It has to be considered that only the transients that reach an equilibrium process can be properly fitted. Those curves that are not saturated after the corresponding oxygen exchange process are not valid for the fitting and, therefore, all the graphs in this work only contain τ values obtained from equilibrium states. Figure 4 displays the temperature dependence of τ values for the out- and in-diffusion processes. The τ values are longer for the out-diffusion process (~7 min at 500 °C to ~0.4 min at 800 °C) than for in-diffusion (~4 min at 400 °C to ~0.5 min at 500 °C). In the case of the in-diffusion, above 500 °C, the process is so fast that it is not possible to obtain an accurate value of τ .

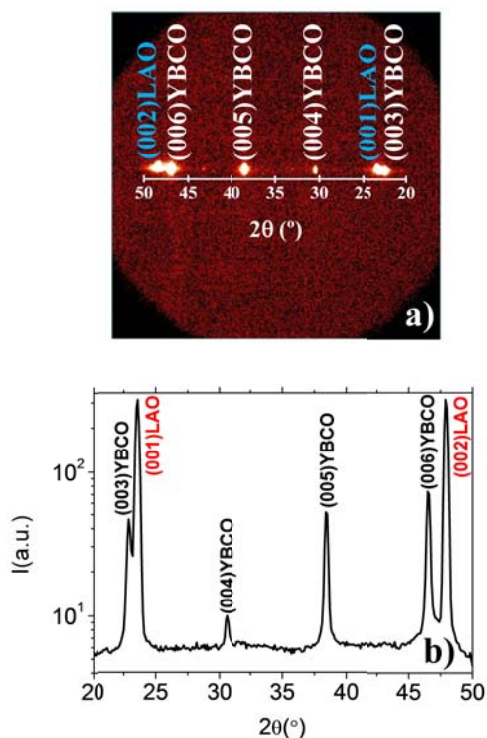


Figure 1. 2D XRD θ - 2θ a) frame and b) integrated patterns of a 250 nm CSD YBCO film studied in this work. The films display a perfect 2D texture.

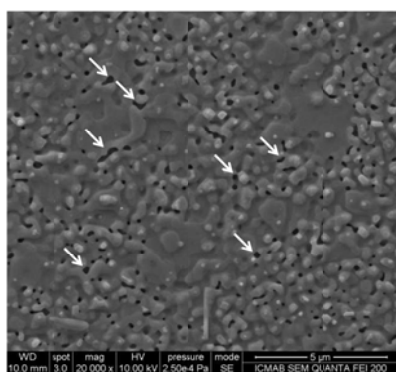


Figure 2. SEM image of a typical 250 nm CSD YBCO film showing a dense and homogeneous surface with presence of some pores (white arrows).

The conductance transients corresponding to oxygen out- and in-diffusion were fitted using equation 6 to find the τ values (Figure 3c)). It is observed that good fits are achieved which correspond either to a process limited by surface reaction or by bulk diffusion,

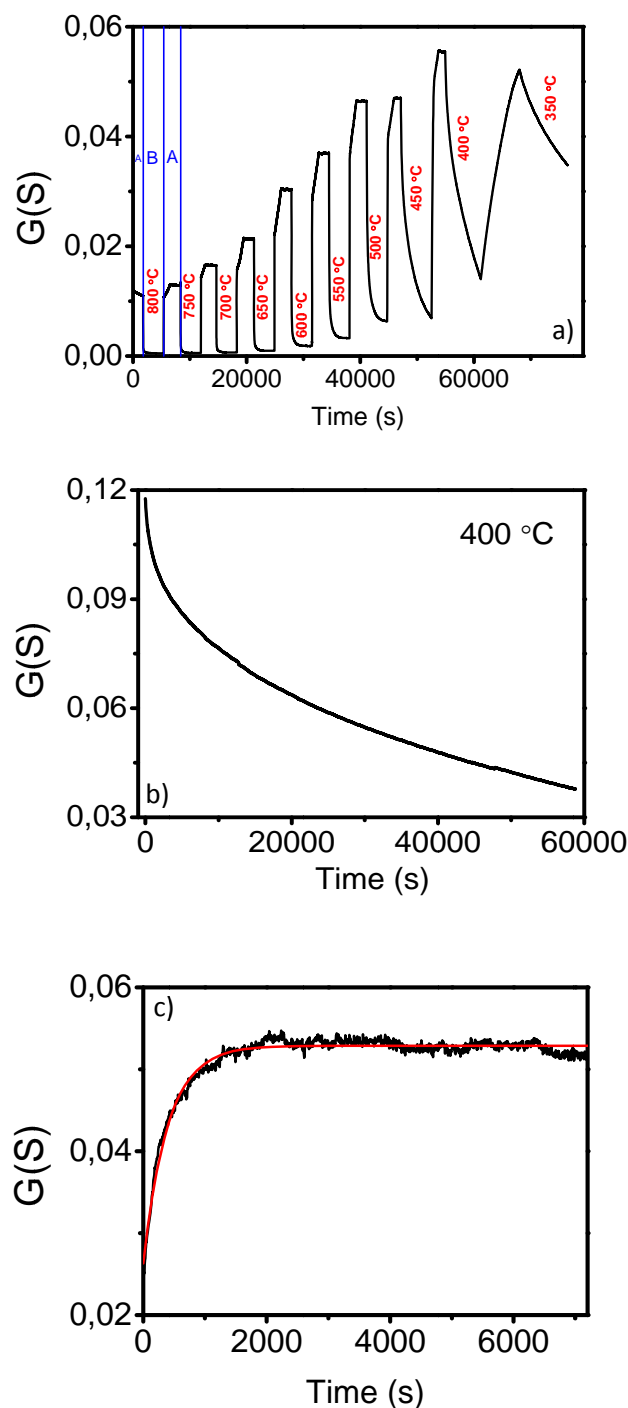


Figure 3. a) Evolution of the conductance with time for different temperatures using alternative changes of PO_2 (A: $P_H=1$ atm and B: $P_L=2 \times 10^{-4}$ atm). b) Example of a non-saturated conductance relaxation measurement made at very long times (15 h) for an out-diffusion process at 400 °C. c) Typical fitting (red curve) of an experimental conductivity relaxation measurement (black curve) using expression (5) to determine the τ values (in-diffusion process at 450 °C).

On the right Y axis of figure 4 the values of the surface reaction rates k_s obtained by application of equation 5 are also indicated.

The log k_s vs. $1/T$ series of points have been fitted to a linear dependence to extract the activation energy, E_a and k_o ($k_s=k_o \exp^{E_a/kT}$). For out-diffusion, it is found $E_a = 0.25 \pm 0.05$ eV in the 550–800 °C range, whereas a much higher value of 0.8 ± 0.2 eV is obtained for in-diffusion E_a in the 400–500 °C range.

The in-diffusion E_a value is similar to those previously reported for sputtered YBCO thin films and bulk and liquid phase epitaxy (LPE) samples^{15,19,47,48} while the E_a value of out-diffusion process is considerably smaller (no similar analyses have been previously reported). The k_o values determined from the intercepts of the straight lines in figure 4 also strongly differ between out- and in-diffusion processes: $k_o = 1.5 \times 10^{-6} \pm 8 \cdot 10^{-7}$ cm/s and 0.29 ± 0.09 cm/s for the out- and in-diffusion processes, respectively.

At this stage we wonder if the asymmetric behavior between out- and in-diffusion processes is real or if it arises from an experimental artifact associated to the conductivity relaxation experiments which might be influenced by different electrical current percolation paths between both experiments^{48,49}. To ensure that this is not the case, we performed thermogravimetric analysis (TGA) experiments on YBCO powders of small particle size (10 μm of diameter) to ascertain if the asymmetry is also observed in this case. We indeed found that under similar conditions of temperature and P_H and P_L values, similar τ values are obtained and the asymmetry is maintained (see figure 5). Hence, we confirm that the asymmetric behavior of oxygen exchange is an intrinsic characteristic of YBCO under the experimental conditions used in our experiments.

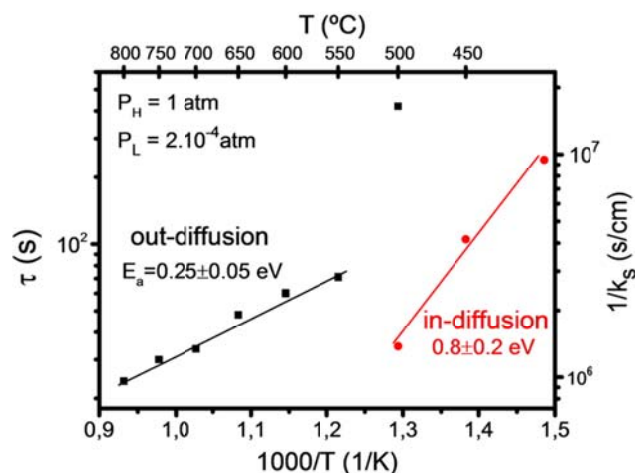


Figure 4. Evolution of τ values with temperature and k_s vs. $1000/T$ curves for the out-diffusion (black) and in-diffusion (red) processes of a 250 nm pristine YBCO film following the PO_2 changes shown in figure 3.

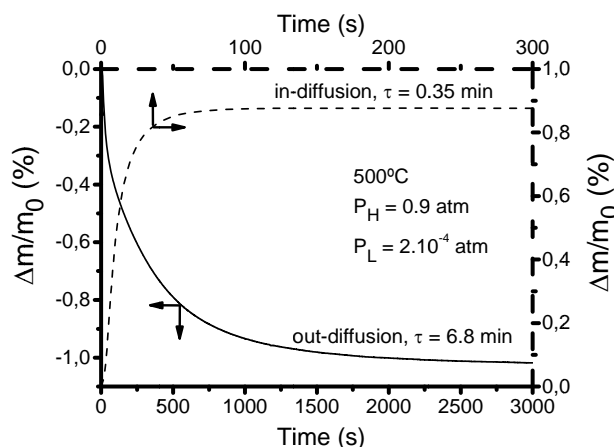


Figure 5. TGA measurements of the mass change due to the oxygen out-diffusion (solid) and in-diffusion (dashed) processes in a YBCO polycrystalline powder sample.

Oxygen pressure dependence of the conductivity relaxation

The oxygen partial pressure PO_2 is a key parameter to analyze the mechanisms limiting the kinetics of the oxygen exchange processes on any oxide. Hence, we have carried out a series of conductance relaxation measurements where P_L was changed within the range $P_L = 5 \times 10^{-5}$ to $P_H = 1$ atm while P_H was kept constant to 1 atm. A first set of experiments was performed to analyze the temperature dependence of τ values at different PO_2 values for out-diffusion processes. The experimental results show that PO_2 has a strong influence on the corresponding τ values (Figure 6).

At higher P_L , τ values are smaller at all temperatures (values shown in Figure 6). Consequently, k_s increases with P_L at all temperatures and it follows a thermally activated behavior whose activation energy depends on PO_2 . E_a has been found to decrease with P_L (Figure 6).

More insight on the influence of PO_2 on the oxygenation kinetics was gained from a second series of experiments where the dependence of τ on P_L was determined by measuring conductance relaxation at 500 °C for both in-diffusion and out-diffusion processes. The procedure is illustrated in figure 7a) where the conductance transients are observed when PO_2 is switched from P_L to P_H and vice versa. Figure 7b) displays the corresponding τ values as a function of P_L . The figure shows that τ follows a power law, i.e., $\tau \propto PO_2^\beta$, with β values differing among in- and out-diffusion processes. Consequently, the corresponding τ values are progressively different when P_L moves away from P_H .

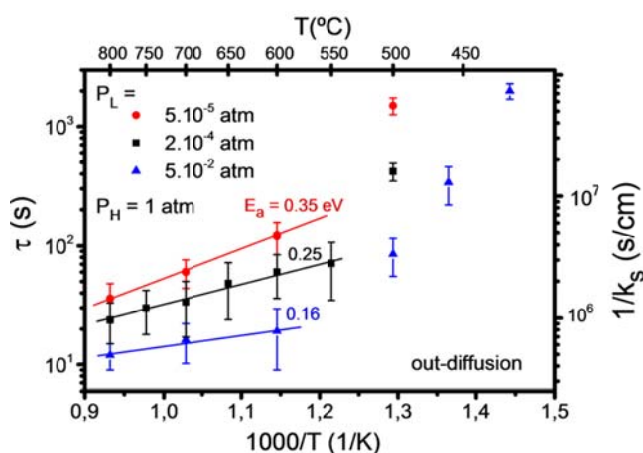


Figure 6. Measurements of the out-diffusion processes showing the evolution of τ values with temperature for different P_L values and $P_H = 1$ atm. Dependence of k_s vs. $1/T$ for different P_L values is also indicated together with the corresponding E_a values.

Actually, the reaction rates of surface reactions usually follow power law dependences PO_2^β , where β depends on each particular reaction. Hence, the conductance relaxation times should also follow such dependence ($\tau \propto PO_2^\beta$) if oxygen exchange is dominated by surface reactions^{29,30,50}. The power law dependences of the reaction rates have a thermodynamic origin derived from the equilibrium constant of the chemical reaction and also from the influence of oxygen adsorbate coverage on PO_2 ^{48,50}. The analysis of the τ power dependence on PO_2 can therefore provide more input into the rds of the surface reactions. It can also further clarify the origin of some controversial observations concerning the possible existence of an asymmetric behavior between in and out-diffusion oxygenation kinetics in YBCO⁵¹⁻⁵⁴. The results reported in figure 7b) draw a plausible scenario for this controversy: in any experimental analysis of the asymmetry issue it is required that P_L and P_H differ in a significant amount to detect the corresponding effects.

At this stage we should stress that bulk diffusion might also introduce some dependence of oxygenation kinetics on PO_2 because the equilibrium oxygen content δ of YBCO depends on PO_2 ⁴², and this brings some dependence on PO_2 to the chemical diffusion constant D , an usual feature in most MIEC oxides⁵⁵⁻⁵⁸. However, in YBCO the dependence of D with δ seems to be rather weak, even if a thorough investigation of this effect in single crystals or epitaxial films would be worthwhile to handle properly the YBCO diffusion constant anisotropy effects^{9,11,15,48,49,59-64}.

The results shown in figures 3 to 7 provide, therefore, an adequate framework to disentangle the corundum of the surface oxygen exchange mechanisms in CSD YBCO films. For instance, the strong divergence between in-diffusion and out-diffusion kinetics (i.e., modified τ values and a strong decrease of E_a for the out-diffusion processes) can only be attributed to the asymmetry of the surface reactions.

An additional parameter which may influence the observed oxygenation kinetic asymmetries is the temperature, so we investigated the τ dependence on P_L at different temperatures. Figure 8 shows that the ratio of τ values for in- and out-diffusion follows a PO_2 power law dependence with β independent of temperature for the investigated temperature range.

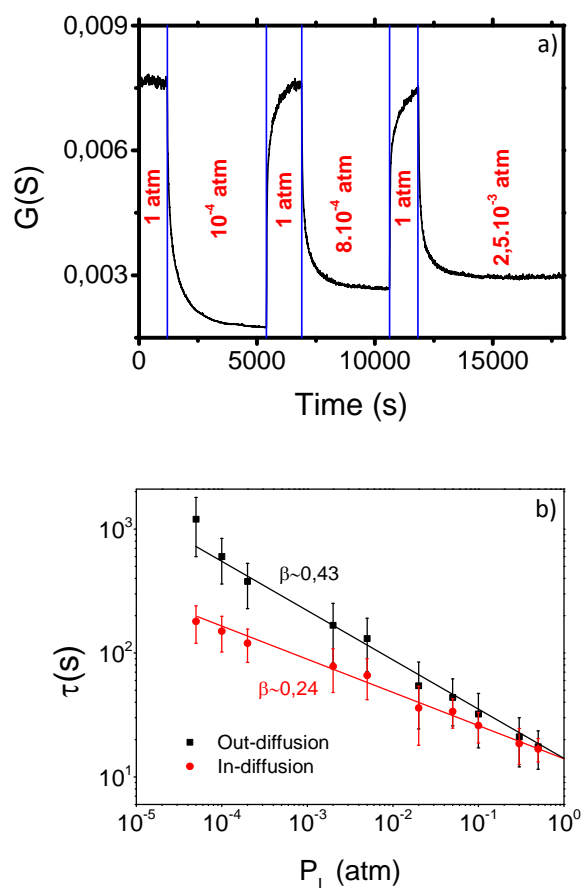


Figure 7. a) Evolution of the electrical conductance with time at 500 °C when different out-and in-diffusion processes are carried out with different P_L values and maintaining constant the $P_H = 1$ atm. b) Evolution of τ values for the in- and out-diffusion processes shown in a). In the in-diffusion and out-diffusion experiments the initial or final P_L values were variable, respectively. The slope of the power law curves indicate that the factor β is $\sim 0.43 \pm 0.04$ for the out-diffusion and $\sim 0.24 \pm 0.05$ for the in-diffusion.

This behavior provides more understanding on the surface reaction processes limiting the oxygen exchange. Since, as commented above, one does not expect an asymmetry in the kinetics of in- and out-diffusion for a process controlled by bulk diffusion, the continuous lines of figure 8 extrapolate to the different P_L values where $\tau_{in}/\tau_{out} \sim 1$, i.e., when the experimental behavior is indistinguishable from that of bulk diffusion. Under these conditions the difference in PO_2 between both processes become very small and the equilibrium states are reached very fast. Our analysis clarifies, therefore, why previous reports in single crystals showed that τ values of in- and out-diffusion were indistinguishable: the departures from the equilibrium were too small^{15,60}. The asymmetric behavior associated to oxygen surface reactions, therefore, can only be detected when large enough PO_2 steps are used.

Finally, we can conclude this section by analyzing in more detail the rds associated to surface reactions from the PO_2 dependence of τ values.

This analysis is mainly grounded on the determination of β exponents which always depend on the particular rds to be

considered. In the case of STO films, Merkle and Maier described in detail the values of the exponent corresponding to each particular surface reaction²⁹. For the case of YBCO films, on the other hand, Chen et al proposed that the β parameter associated to the surface reactions should be $\frac{1}{2}$.¹⁷

In the most complete analysis of these issues, reported by Merkle and Maier for STO films²⁹, a useful approach was to determine the equilibrium reaction rate (R^0) from the τ values of the in- and out-diffusion processes. The following equation was proposed (Equation 6):

$$R^0 \propto \sqrt{k_{s_{in}} k_{s_{out}}} \rightarrow R^0 \propto \sqrt{\frac{1}{\tau_{in} \tau_{out}}} \quad (\text{Equation 6})$$

In the case of STO films, the relationship between R^0 and PO_2 for each step of the surface reactions was described²⁹. These reactions are similar to those proposed by Kuklja et al for the case of (Ba,Sr)(Co,Fe)O_{3-z} films and already mentioned in the introduction²⁵. By representing a log-log plot of the obtained R^0 values vs. P_L for our CSD YBCO films at 500 °C one can determine the coefficient of the power law dependence (Figure 9). The obtained value $\beta \sim 0.34$ suggests, following the proposal for the STO films, that the rds in our case could be either the chemisorption process, leading to the formation of O_2^{2-} molecules from O_2 in the gas phase, or the dissociation of the O_2^{2-} molecule to form two O^- ions on the film surface. We should note, however, that the results obtained here for CSD YBCO films can not be directly compared with the coefficients derived for STO films²⁹. The calculations were made in that case assuming the adsorption equilibrium to be in the limit of low coverage and based on the bulk defect chemical data. Bearing this in mind, it is clear that our identification of the rds in CSD YBCO films can only be considered as a first approximation to a complex problem requiring further theoretical and experimental investigation.

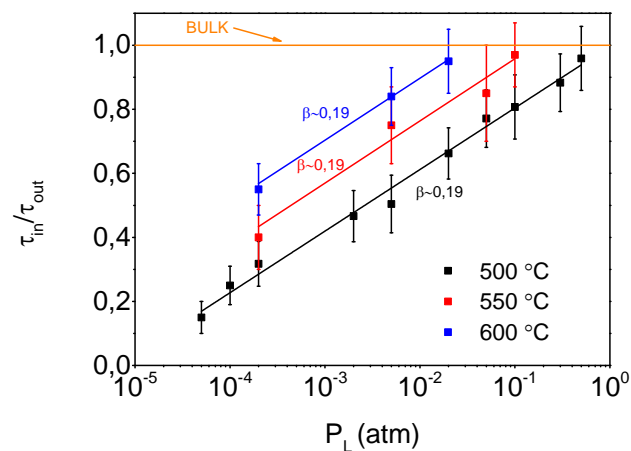


Figure 8. Plot of the ratio of τ values of the in- and out-diffusion at different temperatures vs. P_L , when P_H is fixed at 1 atm, as shown in figure 6.

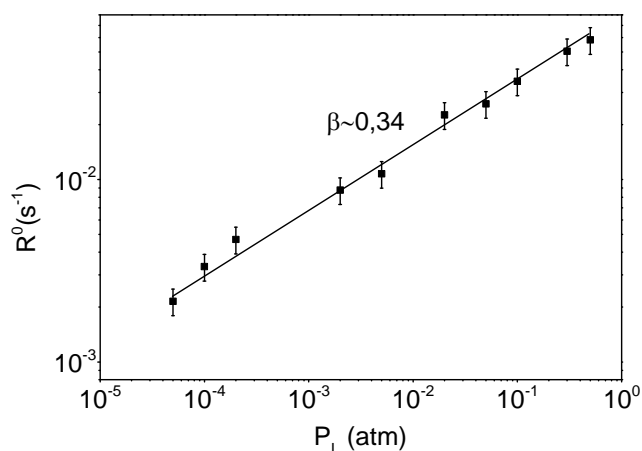


Figure 9. Dependence of the equilibrium reaction rate R^0 on P_L for YBCO CSD films. The observed $P_L^{0.34}$ dependence measured at 500 °C suggests that the rds is linked to the chemisorption or dissociation of the O_2^{2-} molecule.

Use of silver to accelerate the kinetics of the YBCO oxygen exchange

The analysis of the oxygenation kinetics in CSD YBCO films presented up to now has demonstrated that the surface reactions limit the rate of oxygen exchange. It was also found that at low temperatures (below 550 °C and 400 °C for out- and in-diffusion, respectively) the processes are too slow to reach the equilibrium state within the experimental time window. Consequently, it is not possible to carry out oxygenation processes below 400 °C in reasonable times because the oxygen incorporation will be incomplete (Figure 3b)). However, oxygenation at low temperatures would be interesting because one can further modify the oxygen content of the YBCO films^{65–68}. To overcome the low temperature limitation in the oxygenation of functional oxides, it has been shown that silver can be used as a catalyst to enhance the rate of oxygen incorporation. The use of silver as a catalyst for selective oxidation processes is well-known in different fields, especially in the hydrocarbon industry^{69,70}. Additionally, it has excellent oxygen solubility and permeability, two critical properties to achieve a fast oxygen exchange⁷¹. The role of silver is to facilitate the O_2 molecules dissociation and reduction. When an O_2 molecule is adsorbed in a silver surface, there is an electron transfer from silver to the π^* orbitals of the O_2 molecules. This causes a decrease in the binding energy of the O=O bond facilitating its rupture⁷². This strategy was successfully tested in STO films²⁸. A layer of silver (100 nm) was deposited on top of STO by sputtering. After an annealing process of 7 days at 1023 K the silver layer transforms into micro/nanoparticles on the STO surface. The STO films with these silver nanoparticles on the top showed lower E_a and also much higher k_0 values than the pristine samples²⁸.

In our case we have introduced silver either directly in the YBCO solution or as evaporated metallic layers, on the YBCO surface. In the first case a YBCO+5%M Ag solution is prepared by adding Ag-TFA salt to the YBCO solution and the films were synthesized using similar growth processes than in pristine YBCO films. The structure and superconducting properties are similar to the previously investigated films⁷³. Silver shows a tendency to diffuse towards the films surface before its sublimation and, at 810 °C, some traces of

silver remain in the surface (at 720 °C some silver NPs are still detected at the surface after growth)⁷³.

In the case of Ag coating of the YBCO films its typical initial thickness is ~100 nm, however, after thermal annealing at 300 °C for about 5 h, the typical surface microstructure corresponds to that of nanometric or micrometric Ag particles (Figure S2 in SI). Conductivity relaxation experiments, both for the out- and in-diffusion processes, have been performed in these films at temperatures below 350 °C where the pristine YBCO films displayed very long oxygenation times. A comparison of the typical conductance relaxation at 350 °C and 300 °C of pristine and YBCO-Ag coated films is shown in figures 10a) and 10b). It can be observed that the equilibrium oxygenation in YBCO-Ag coated films is reached within reasonable oxygenation times while in pristine YBCO films saturation is not reached, even after times as long as 12–15 h (Figure 3b)).

These results demonstrate that the oxygenation kinetics is much faster when Ag is deposited on the films surface.

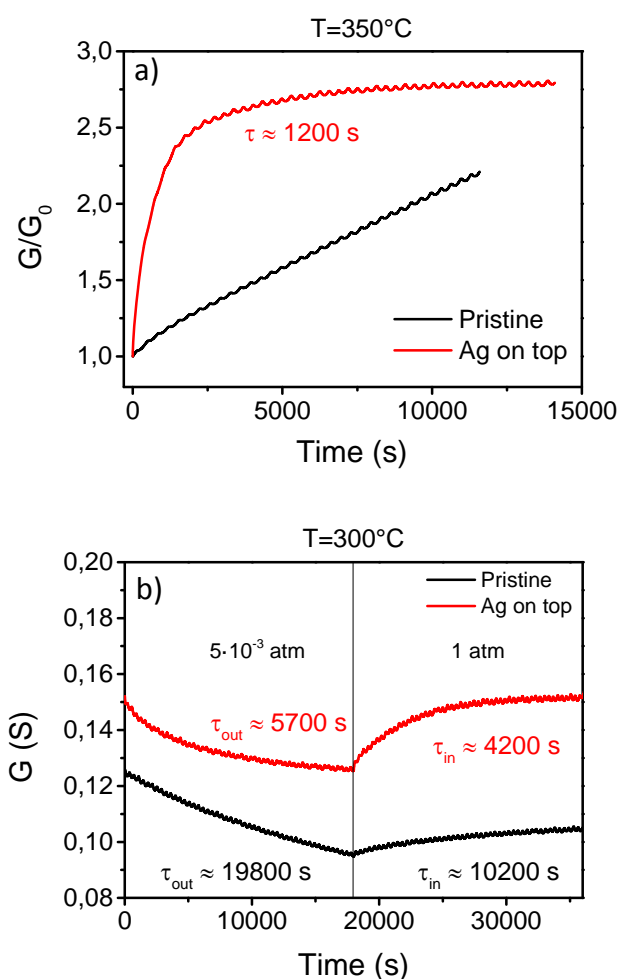


Figure 10. a) Conductance relaxation due to an in-diffusion process originated by a PO_2 step from $P_L=5 \times 10^{-3}$ atm to $P_H=1$ atm in pristine and YBCO-Ag coated films at 350 °C. The difference in the oxygen exchange rate among both types of films is clearly observed. b) Evolution of the conductance during in- and out-diffusion processes at 300 °C with $P_L=5 \times 10^{-3}$ atm and $P_H=1$ atm. The corresponding τ values are also indicated.

It is clear that oxygen in-diffusion is favored at low temperatures by silver. When silver is on the surface of the YBCO, the number of O₂ molecules that are adsorbed and dissociated is larger due to the reduction of the bond energy and, probably, also due to an enhanced sticking probability of the molecules. It has been suggested that oxygen atoms diffuse into bulk silver and reach the films surface. This oxygen path was proposed for a silver membrane kept at temperatures above 310 °C. Below this temperature, the atomic oxygen is found to be locked at the silver surface without diffusion into the silver layer⁷⁴⁻⁷⁶. The overall result of this phenomenon is the acceleration of the surface reactions. Probably silver is able to accelerate the rds, which was suggested to be the dissociation of the O₂⁻ molecule (or the formation of O₂²⁻). A thorough analysis of the temperature and PO₂ dependence of these films will be required to properly analyze the microscopic mechanisms responsible of such a strong modification of the oxygen exchange processes.

Discussion

The results presented in the previous sections have provided compelling evidence of the oxygen surface exchange reactions as the limiting step in the oxygenation processes of CSD YBCO films. In other words, the surface reactions are slower than the bulk diffusion process in these thin films. It is an useful exercise, however, to compare the surface reaction rates to the expected bulk diffusion rates in YBCO crystals. For this purpose we need to take into account that along the a-b planes the bulk oxygen diffusion coefficient is much larger than the diffusion constant along the c-axis ($D_{ab} \approx 10^6 D_c$)⁹. Since volume diffusion is faster than the surface oxygen surface exchange, we can estimate from our data an upper bound of the oxygen diffusion length parallel to the ab planes, based on previously determined chemical diffusion constants.

A comparative analysis of oxygenation rates in bulk melt textured ceramics and thin films has been performed previously, where it was assumed that bulk oxygen diffusion was the limiting step. The determination of an upper bound of the grain size (or diffusion length) can be made using the following formula (Equation 7)¹⁵:

$$L = \sqrt{2\pi^2\tau D_{ab}} \quad (\text{Equation 7})$$

With the experimental τ values for the oxygen in-diffusion process at 700 °C in our CSD films L is estimated to be in the range of $L \sim 0.3\text{--}0.7 \mu\text{m}$, depending on the D_{ab} values chosen in the calculation. The diffusion lengths estimated by other authors for different YBCO samples from their experimental τ values were: $L \sim 10^3\text{--}10^4 \mu\text{m}$ for melt textured bulk ceramics YBCO¹⁹, $L \sim 10^1\text{--}10^2 \mu\text{m}$ for LPE films⁴⁷ or $L \sim 0.2 \mu\text{m}$ for sputtered films^{15,60}. The upper bound of our CSD films is therefore similar to the values previously reported for sputtering films.

Figure 11 compares typical $\ln(1/\tau)$ vs. $1000/T$ curves for the oxygen in-diffusion process of the above mentioned YBCO samples. It is observed that the CSD film curve is situated at the top left part, thus indicating that the τ values are the smallest in this range of temperatures. The E_a values for the in-diffusion process of the CSD films are similar to those found in LPE, sputtering or bulk ceramics. In the case of CSD YBCO films, the values vary in the range 0.8–1 eV, which are similar to the previously reported values (1.1–1.25 eV) in other types of samples. For the out-diffusion processes, however,

as we mentioned before, the E_a values are reduced to $E_a = 0.2\text{--}0.3$ eV, thus pointing towards a modified rds mechanism^{22,77}, or an asymmetry of the surface reactions during oxygen exchange⁴⁸.

Concerning the observed τ_0 values in Figure 11, the obtained results for each technique are quite different. The τ_0 values for CSD and sputtering films are in the range of $10^{-5}\text{--}10^{-7}$ s while in the case of the LPE and MTG samples the τ_0 values are in the range of $10^{-2}\text{--}10^{-3}$ s, a reflect of the larger L values in these materials. We suggest therefore that in YBCO films with a thickness in the range of hundreds of nanometers and with small grain sizes (below $\sim 1 \mu\text{m}$), or a high concentration of pores or defects, the surface reactions are the rate limiting factor for oxygen exchange. When the sample thickness increases above several micrometers and the grain sizes also increases, as in the case of the LPE samples ($10 \mu\text{m}$ of thickness with large grains of $10^1\text{--}10^2 \mu\text{m}$), the rate limiting factor is bulk diffusion.

The microscopic mechanisms underlying the obtained E_a values arise actually from different sources, depending if bulk diffusion or surface exchange is the rds. In the case of bulk controlled mechanisms the E_a correspond to the energy barrier that the oxygen ions have to overcome to diffuse inside the YBCO structure. On the other hand, the E_a values in a surface controlled mechanism arise from one of the energy barriers that the oxygen molecules have to overcome: chemisorption, diffusion or dissociation.

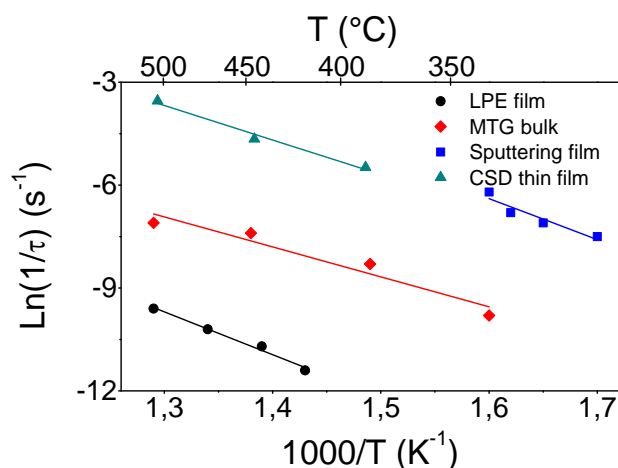


Figure 11. In-diffusion $\ln(1/\tau)$ vs. $1000/T$ curves for the YBCO LPE films⁴⁷, sputtering films^{15,60}, MTG bulk samples¹⁹ and CSD films.

After reaching the conclusion that oxygen diffuses along lengths shorter than $0.3\text{--}0.7 \mu\text{m}$, we may wonder if these are reasonable values taking into account the microstructure of the CSD films. Actually, the scenario suggested for the present CSD YBCO films is quite similar to that previously suggested by other authors for epitaxial functional oxide films^{17,18,78}. These works proposed that the oxygen exchange in epitaxial films takes place through two different exchange channels: the native surface and the dislocations usually present in the films. The claim is that the oxygen exchange rate through these two channels strongly differs. Oxygen diffusion through the dislocations is much faster than through the native surface because in defective structures the oxygen mobility is higher^{79,80} and the number of oxygen vacancies is larger than in the bulk^{79,81}, thus enhancing the bulk diffusion.

In the case of the CSD YBCO films we propose a slightly modified scenario. First, the surface reactions are completed at the native surface. In the case of YBCO films grown by CSD, no threading

dislocations exist even at very low thicknesses⁸², so it is considered that oxygen ion exchange towards the bulk of the film happens mainly through pores or low angle grain boundaries. Actually, as it is observed in figure 3, the density of pores in the 250 nm thick CSD YBCO films is quite high while grain boundaries in CSD YBCO films have also been shown to play some role in the transport properties and so they are probably also active as fast oxygen diffusion paths^{48,52,83}. We propose, therefore, that oxygen ions penetrate into the films along the vertical direction through these pores, where the surface reactions may also occur, as well as along the low angle grain boundaries remaining in the CSD epitaxial films^{54,59}. These oxygen exchange paths should be much faster than bulk diffusion along the *c*-axis within the bulk of the film due to the low values of D_c mentioned before. Actually, we estimate that oxygen ions can diffuse over a distance between 300 and 700 times longer along *a*-*b* planes than along the *c*-axis. We should note here that the mean separation distance between pores is at least as small as the diffusion length, *L*, calculated through equation 7. Therefore, oxygen ions can diffuse fast enough along the *a*-*b* planes to achieve a homogeneous distribution.

Summarizing, in-diffusion of oxygen proceeds through the five steps indicated in figure 12, four of them linked to the surface reactions and the last one linked to bulk diffusion. First, the O₂ molecules are chemisorbed to the free surface. Then the ionized molecules diffuse into existing defects and they dissociate leading to O²⁻ ions which then require further surface diffusion to find available oxygen vacancies⁸⁴. Once the oxygen molecules complete the surface reactions, if the resulting ions are near a pore, they diffuse through it in the vertical direction and then along the *a*-*b* plane (Figure 12). Molecular oxygen may probably also diffuse within the pores where the surface reactions can be also completed. Anyway, considering the vertical diffusion through the pores or grain boundaries is the only way to justify the observed small τ values.

This scenario is compatible with the reported experimental results and it also clarifies the role of the silver nanoparticles at the surface. At low temperatures, when the oxygen exchange through pores and grain boundaries is still effective, the exchange rate is too small because the rds has been slowed down. When some silver nanoparticles are deposited on the film surface they accelerate the oxygen surface reactions, and probably the oxygen ions surface chemisorption as well. The huge τ values observed in pristine films at low temperatures are then strongly reduced and the conductivity transients become measurable. Essentially, the catalytic effect of silver nanoparticles accelerates the molecular oxygen dissociation reactions in the native surface thus increasing the formation rate of O²⁻ ions at low temperatures and hence enhancing the efficiency of the oxygen exchange channels to diffuse towards the bulk of the films.

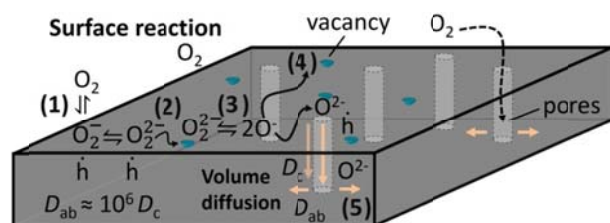


Figure 12. Complete picture of the oxygen exchange process in CSD YBCO films including the surface reactions and the bulk/volume

diffusion. The complete process follows these steps: 1) Chemisorption of the O₂ molecule, 2) surface diffusion to find a vacancy, 3) dissociation of O₂ molecules, 4) the second ion migrate to another vacancy and 5) volume diffusion.

Conclusions

This work was devoted to the study of oxygen in-corporation and ex-corporation processes in CSD YBCO films in order to clarify the limiting factors of the oxygen exchange in this kind of films and we have unequivocally proved that the surface reactions are the limiting factor in the kinetics of the oxygen exchange processes in CSD YBCO films. The PO₂ dependence of conductance relaxation times and the asymmetric behavior of the in- and out-diffusion processes cannot be explained without consideration of oxygen exchange as a surface controlled process. We could also infer, through the study of the PO₂ influence in the relaxation times, which is the rate determining step (rds). We suggest that the chemisorption process leading to the formation of ionized O₂⁻ molecules, or the dissociation of the O₂⁻ molecule to form two O⁻ ions at the surface, is the rds in the present case. Finally, we have also shown that silver is an effective catalytic agent to accelerate the rate of the oxygen exchange rates at lower temperatures than those we can achieve in pristine YBCO films. The reduction of relaxation times in Ag coated YBCO films was quite significant at low temperatures, thus allowing to shorten the oxygenation times of the films at low temperatures where the pristine films can not be fully oxygenated. It is suggested that silver reduces the strength of O=O bond and decreases drastically the overall surface reaction times. After completing the surface reactions, the oxygen ions diffuse parallel to the *ab* planes into the volume of the films profiting of the existing pores and grain boundaries.

Experimental

The films studied in this work were prepared by CSD following the trifluoroacetate (TFA) route. YBCO metallorganic precursor solutions based on anhydrous TFA salts were prepared and characterized as described in detail previously^{73,85}. Basically, YBCO solid ceramic powder is dissolved in trifluoroacetic acid, trifluoroacetic anhydride and acetone. Further, the mixture is purified to finally obtain a 0.25M (with respect to the Y content) YBCO-TFA solution. Alternative YBCO+5% mol Ag solutions are prepared by adding the corresponding stoichiometric amount of Ag-TFA precursor salts to the original 0.25M YBCO-TFA solution. These solutions were deposited by spin-coating on 5×5mm² LaAlO₃ (001) (LAO) substrates. The subsequent pyrolysis and growth processes are also described elsewhere^{85–87}. The phase analysis of the YBCO films was done by X-ray diffraction using a Bruker AXS GADDS diffractometer equipped with a 2D detector. The morphology of the fully grown films was studied to observe the presence of precipitates, porosity and the degree of grain disorientation. The Scanning Electron Microscopy (SEM) images were obtained with a SEM Quanta 200 ESEM FEG equipment.

The films conductance was determined by electrical measurements carried out with a standard system reported elsewhere^{17,18,87,88}. It consists of a 4-probe contact in a Van der Pauw configuration. The sample is held in the center of a 22 mm furnace tube that allows to control the temperature and gas atmosphere. All experiments have been done at atmospheric pressure. The PO₂ was set by mixing N₂ and O₂ with appropriate mass-flow meters. The in-diffusion conductance transients were measured after PO₂ was switched from a low-value, P_L, to a high value, P_H; and the reverse was done for the out-diffusion experiments.

The influence of the gas flow on the oxygen exchange kinetics was analyzed for out-diffusion experiments in order to evaluate the proper flow to be used in all the kinetic experiments. Out-diffusion experiments were

performed at gas flows in the range 0.15 to 0.6 l/min at different temperatures (300–800 °C) (Figure S1 in Supporting Information (S.I.)). It was found that some dependence on gas flow exists which is enhanced at low temperatures and which tends to stabilize at 0.6 l/min. This gas flow dependence at low gas flow rates arises probably from insufficient oxygen diffusion across the boundary layer formed on top of the films. For this reason all the reported experiments were performed under the highest gas flow allowed in our experimental set up, i.e., 0.6 l/min.

Acknowledgements

Authors acknowledge the MICIN (NANOSELECT, CSD2007-00041 and MAT2014-51778- C2-1-R and C2-2-R), Generalitat de Catalunya (2014SGR 753 and Xarmae), and the EU (EU-FP7 NMP-LA-2012-280432 EUROTAPES project, Cost Action MP1201) and ERC ADG-2014-669504. M.C. is grateful to MINECO for the “Ramon y Cajal” contract RYC-2013-12448. They also acknowledge MINECO for the Center of Excellence award Severo Ochoa (SEV-2015-0496). C.F. Sánchez-Valdés acknowledges the support received from CSIC under JAE-Predocctorals program. We also acknowledge useful discussions with Dr. S. Ricart.

References

- X. Obradors and T. Puig, *Supercond. Sci. Technol.* **27**, 44003 (2014).
- X. Obradors, T. Puig, A. Pomar, F. Sandiumenge, N. Mestres, M. Coll, A. Cavallaro, N. Romà, J. Gázquez, J. C. González, O. Castaño, J. Gutiérrez, A. Palau, K. Zalamova, S. Morlens, A. Hassini, M. Gubert, S. Ricart, J. M. Moretó, S. Piñol, D. Isfort and J. Bock, *Supercond. Sci. Technol.* **19**, S13–S26 (2006).
- X. Obradors, T. Puig, A. Pomar, F. Sandiumenge, S. Piñol, N. Mestres, O. Castaño, M. Coll, A. Cavallaro, A. Palau, J. Gázquez, J. C. González, J. Gutiérrez, N. Romà, S. Ricart, J. M. Moretó, M. D. Rossell and G. van Tendeloo, *Supercond. Sci. Technol.* **17**, 1055–1064 (2004).
- T. Izumi, M. Yoshizumi, J. Matsuda, K. Nakaoka, Y. Kitoh, Y. Sutoh, T. Nakanishi, A. Nakai, K. Suzuki, Y. Yamada, A. Yajima, T. Saitoh and Y. Shiohara, *Phys. C Supercond. its Appl.* **463**, 510–514 (2007).
- Y. Shiohara, T. Taneda and M. Yoshizumi, *Jpn. J. Appl. Phys.* **51**, 10007 (2012).
- Y. Shiohara, M. Yoshizumi, Y. Takagi, T. Izumi, *Phys. C Supercond.* **484**, 1–5 (2013).
- S. Tsukui, R. E. Koritala, M. Li, K. C. Goretta, M. Adachi, J. E. Baker, J. L. Routbort, *Phys. C Supercond.* **392**, 841–846 (2003).
- R. Mogilevsky, R. Levi-Setti, B. Pashmakov, L. Liu, K. Zhang, H. M. Jaeger, D. B. Buchholz, R. P. H. Chang and B. W. Veal, *Phys. Rev. B* **49**, 6420–6423 (1994).
- S. J. Rothman, J. L. Routbort, U. Welp and J. E. Baker, *Phys. Rev. B* **44**, 2326–2333 (1991).
- T. B. Tang and W. Lo, *Phys. C Supercond.* **174**, 463–466 (1991).
- K. Kishio, K. Suzuki, T. Hasegawa, T. Yamamoto, K. Kitazawa and K. Fueki, *J. Solid State Chem.* **82**, 192–202 (1989).
- A. Michaelis, E. A. Irene, O. Auciello and A. R. Krauss, *J. Appl. Phys.* **83**, 7736 (1998).
- G. S. Grader, P. K. Gallagher, J. Thomson, and M. Gurvitch, *Appl. Phys. A Solids Surfaces* **45**, 179–183 (1988).
- S. H. Lee, S. C. Bae, J. K. Ku and H. J. Shin, *Phys. Rev. B* **46**, 9142–9146 (1992).
- S. Kittelberger, U. Bolz, R. P. Huebener, B. Holzapfel and L. Mex, *Phys. C Supercond.* **302**, 93–101 (1998).
- C. Krauns and H. -U. Krebs, *Zeitschrift für Phys. B Condens. Matter* **92**, 43–46 (1993).
- L. Chen, C. L. Chen and A. J. Jacobson, *IEEE Trans. Applied Supercond.* **13**, 2882–2885 (2003).
- T. Qu, Y. Xue, F. Feng, R. Huang, W. Wu, K. Shi and Z. Ha, *Phys. C Supercond.* **494**, 148–152 (2013).
- H. Zhang, H. Ye, K. Du, X. Y. Huang and Z. H. Wang, *Supercond. Sci. Technol.* **15**, 317 (2002).
- A. Fick, *Ann. der Phys. und Chemie* **170**, 59–86 (1855).
- A. Fick, *London, Edinburgh Dublin Philos. Mag. J. Sci.* **10**, 30–39
- S. B. Adler, *Chem. Rev.* **104**, 4791–4844 (2004).
- S. B. Adler, X. Y. Chen and J. R. Wilson, *J. Catal.* **245**, 91–109 (2007).
- A. J. Jacobson, *Chem. Mater.* **22**, 660–674 (2010).
- M. M. Kuklja, E. A. Kotomin, R. Merkle, Yu. A. Mastrikov and J. Maier, *Phys. Chem. Chem. Phys.* **15**, 5443 (2013).
- M. V. Ananyev, E. S. Tropin, V. A. Eremin, A. S. Farlenkov, A. S. Smirnov, A. A. Kolchugin, N. M. Porotnikova, A. V. Khodimchuk, A. V. Berenov and E. Kh. Kurumchin, *Phys. Chem. Chem. Phys.* **18**, 9102–9111 (2016).
- C. Körber, A. Wachau, P. Ágoston, K. Albe and A. Klein, *Phys. Chem. Chem. Phys.* **13**, 3223 (2011).
- M. Leonhardt, R. A. De Souza, J. Claus and J. Maier, *J. Electrochem. Soc.* **149**, J19 (2002).
- R. Merkle and J. Maier, *Phys. Chem. Chem. Phys.* **4**, 4140–4148 (2002).
- R. Merkle and J. Maier, *Angew. Chemie Int. Ed.* **47**, 3874–3894 (2008).
- L. Wang, R. Merkle and J. Maier, *J. Electrochem. Soc.* **157**, B1802 (2010).
- V. Metlenko, W. Jung, S. R. Bishop, H. L. Tuller and R. A. De Souza, *Phys. Chem. Chem. Phys.* **18**, 29495–29505 (2016).
- Z. A. Feng, F. El Gabaly, X. Ye, Z.-X. Shen and W. C. Chueh, *Nat. Commun.* **5**, (2014).
- A. Karthikeyan and S. Ramanathan, *Appl. Phys. Lett.* **92**, 243109 (2008).
- Y. Shi, A. H. Bork, S. Schweiger and J. L. M. Rupp, *Nat. Mater.* **14**, 721–727 (2015).
- S. V. Kalinin, A. Borisevich and D. Fong, *ACS Nano* **6**, 10423–10437 (2012).
- A. Sawa, *Mater. Today* **11**, 28–36 (2008).
- C. Moreno, C. Munuera, S. Valencia, F. Kronast, X. Obradors and C. Ocal, *Nano Lett.* **10**, 3828–3835 (2010).
- N. Knoblauch, L. Dörrer, P. Fielitz, M. Schmücker and G. Borchardt, *Phys. Chem. Chem. Phys.* **17**, 5849–5860 (2015).
- J. L. Routbort and S. J. Rothman, *J. Appl. Phys.* **76**, 5615 (1994).
- J. Crank, *The mathematics of diffusion*. (Clarendon Press, 1975).
- J. Shimoyama, S. Horii, K. Otszchi, K. Kishio, *MRS Proc.* **2001**, 689, E8.18.
- E. D. Specht, C. J. Sparks, A. G. Dhere, J. Brynstad, O. B. Cavin, D. M. Kroege and H. A. Oye, *Phys. Rev. B* **1988**, 37 (13).
- J. Ye and K. Nakamura, *Phys. Rev. B* **1993**, 48 (10).
- R. Liang, D. A. Bonn and W. N. Hardy, *Phys. Rev. B* **2006**, 73 (18), 180505.
- T. B. Lindemer, J. F. Hunley, J. E. Gates, A. L. Sutton, J. Brynstad, C. R. Hubbard and P. K. Gallagher, *J. Am. Ceram. Soc.* **1989**, 72 (10), 1775–1788.
- H. Zhang, X. Yao and X. Zeng, *Phys. status solidi* **201**, 2305–2311 (2004).
- K. Conder, *Mater. Sci. Eng. R Reports* **32**, 41–102 (2001).
- N. K. Tu, N. C. Yeh, S. I. Park and C. C. Tsuei, *Phys. Rev. B* **39**, 304–314 (1989).

50. Y. A. Mastrikov, R. Merkle, E. Heifets, E. A. Kotomin and J. Maier, *J. Phys. Chem. C* **114**, 3017–3027 (2010).
51. J. R. LaGraff and D. A. Payne, *Phys. Rev. B* **47**, 3380–3390 (1993).
52. J. R. LaGraff and D. A. Payne, *Phys. C Supercond.* **212**, 470–477 (1993).
53. J. R. LaGraff and D. A. Payne, *Phys. C Supercond.* **212**, 478–486 (1993).
54. J. R. LaGraff and D. A. Payne, *Phys. C Supercond.* **212**, 487–496 (1993).
55. M. Sjøgaard, P. Vang Hendriksen and M. Mogensen, *J. Solid State Chem.* **180**, 1489–1503 (2007).
56. I. Yasuda and M. Hishinuma, *J. Solid State Chem.* **123**, 382–390 (1996).
57. J. A. Lane and J. A. Kilner, *Solid State Ionics* **136**, 927–932 (2000).
58. D. Rupasov, T. Makarenko and A. J. Jacobson, *J. Solid State Ionics* **265**, 68–72 (2014).
59. M. D. Vázquez-Navarro, A. Kursumovic and J. E. Evetts, *Supercond. Sci. Technol.* **12**, 1117–1122 (1999).
60. S. Kittelberger, O. M. Stoll and R. P. Huebener, *Supercond. Sci. Technol.* **11**, 744–750 (1998).
61. S. Elschner, W. Becker, H. Bestgen and M. Brand, *Phys. C Supercond.* **202**, 401–407 (1992).
62. A. Erb, B. Greb and G. Müller-Vogt, *Phys. C Supercond. its Appl.* **259**, 83–91 (1996).
63. S. Kittelberger, U. Bolz, R.P. Huebener, B. Holzapfel, L. Mex and R.A. Schwarzer, *Phys. C Supercond.* **312**, 7–20 (1999).
64. M. Burriel, H. Téllez, R. J. Chater, R. Castaing, P. Veber, M. Zaghrioui, T. Ishihara, J. A. Kilner and J.-M. Bassat, *J. Phys. Chem. C* **120**, 17927–17938 (2016).
65. J. L. Tallon, *IEEE Trans. Appl. Supercond.* **25**, 1–6 (2015).
66. E. F. Talantsev, S. C. Wimbush, N. M. Strickland, J. A. Xia, P. D'Souza, J. G. Storey, J. L. Tallon, B. Ingham, R. Knibbe and N. J. Long, *IEEE Trans. Appl. Supercond.* **23**, 7200205–7200205 (2013).
67. G. Deutscher, *APL Mater.* **2**, 96108 (2014).
68. G. Deutscher, *J. Appl. Phys.* **111**, 112603 (2012).
69. G. Ertl, *Handbook of heterogeneous catalysis*. (Wiley-VCH, 2008).
70. R. A. Van Santen and H. P. C. E. Kuipers, *Adv. Catal.* **35**, 265–321 (1987).
71. C. C. Yu, J. D. Baek, C. H. Su, L. Fan, J. Wei, Y. C. Liao and P. C. Su, Inkjet-Printed Porous Silver Thin Film as a Cathode for a Low-*ACS Appl. Mater. Interfaces* **8**, 10343–10349 (2016).
72. S. T. Oyama, *Mechanisms in homogeneous and heterogeneous epoxidation catalysis*. (Elsevier, 2008).
73. X. Obradors, F. Martínez-Julián, K. Zalamova, V. R. Vlad, A. Pomar, A. Palau, A. Llordés, H. Chen, M. Coll, S. Ricart, N. Mestres, X. Granados, T. Puig and M. Rikel, *Phys. C Supercond.* **482**, 58–67 (2012).
74. C. Backx, C. P. M. De Groot and P. Biloen, *Surf. Sci.* **104**, 300–317 (1981).
75. V. I. Bukhtiyarov, V. V. Kaichev and I. P. Prosvirin, *J. Chem. Phys.* **111**, 2169 (1999).
76. B. A. Sexton and R. J. Madix, *Chem. Phys. Lett.* **76**, 294–297 (1980).
77. J. Liu, G. Collins, M. Liu and C. Chen, *APL Mater.* **1**, 31101 (2013).
78. L. Yan and P. A. Salvador, *ACS Appl. Mater. Interfaces* **4**, 2541–2550 (2012).
79. K. Szot, W. Speier, G. Bihlmayer and R. Waser, *Nat. Mater.* **5**, 312–320 (2006).
80. K. Otsuka, A. Kuwabara, A. Nakamura, T. Yamamoto, K. Matsunaga and Y. Ikuhara, *Appl. Phys. Lett.* **82**, 877 (2003).
81. R. F. Klie, W. Walkosz, G. Yang and Y. Zhao, *J. Electron Microsc. (Tokyo)* **58**, 185–191 (2009).
82. J. Gázquez, M. Coll, N. Romà, F. Sandiumenge, T. Puig and X. Obradors, *Supercond. Sci. Technol.* **25**, 65009 (2012).
83. V. Solovyov, I. K. Dimitrov and Q. Li, *Supercond. Sci. Technol.* **26**, 13001 (2013).
84. S. K. R. S. Sankaranarayanan and S. Ramanathan, *J. Phys. Chem. C* **114**, 6631–6639 (2010).
85. N. Romà, S. Morlens, S. Ricart, K. Zalamova, J. M. Moretó, A. Pomar, T. Puig and X. Obradors, *Supercond. Sci. Technol.* **19**, 521–527 (2006).
86. X. Obradors, T. Puig, S. Ricart, M. Coll, J. Gázquez, A. Palau and X. Granados, *Supercond. Sci. Technol.* **25**, 123001 (2012).
87. C. F. Sánchez-Valdés, T. Puig and X. Obradors, *Supercond. Sci. Technol.* **28**, 24006 (2015).
88. H. Chen, K. Zalamova, A. Pomar, X. Granados, T. Puig and X. Obradors, *J. Mater. Res.* **25**, 2371–2379 (2010).

Supporting Information

Untangling surface oxygen exchange effects in $\text{YBa}_2\text{Cu}_3\text{O}_{6+x}$ thin films by electrical conductivity relaxation

P. Cayado^a, C. F. Sánchez-Valdés^a, A. Stangl^a, M. Coll^a, P. Roura^b, A. Palau^a, T. Puig^a and Xavier Obradors^{a,*}

Figure S1). The influence of the gas flow on the oxygen diffusion kinetics for the out-diffusion process. Figure a) shows the evolution of the oxygen exchange relaxation time (τ) for the out diffusion process with the gas flow at different temperatures. It is observed that τ reduces at any temperature as the gas flow increases. Figure b) demonstrates that, as the gas flow increases, the differences in τ for different temperatures are reduced so approaching to the equilibrium state. Therefore, it is important to carry out the experiments at high gas flows to maintain the boundary layer in equilibrium with the ambient and avoid local changes in the oxygen partial pressure that can modify locally the diffusion processes.

Figure S2). SEM images of a YBCO film with a silver coating and corresponding EDX analysis of a typical microparticle observed in the image. A uniform coating of 100 nm Ag was achieved by sputtering, however, after thermal annealing at 300 °C for about 5 h the Ag films has been transformed to a discontinuous coating of micro/nanoparticles. Figure a) shows the Ag micro and nanoparticles formed after annealing the Ag coated film at 500 °C for about 5 h. Figures b) and c) show EDX measurements of a selected microparticle which confirms the composition as Ag.

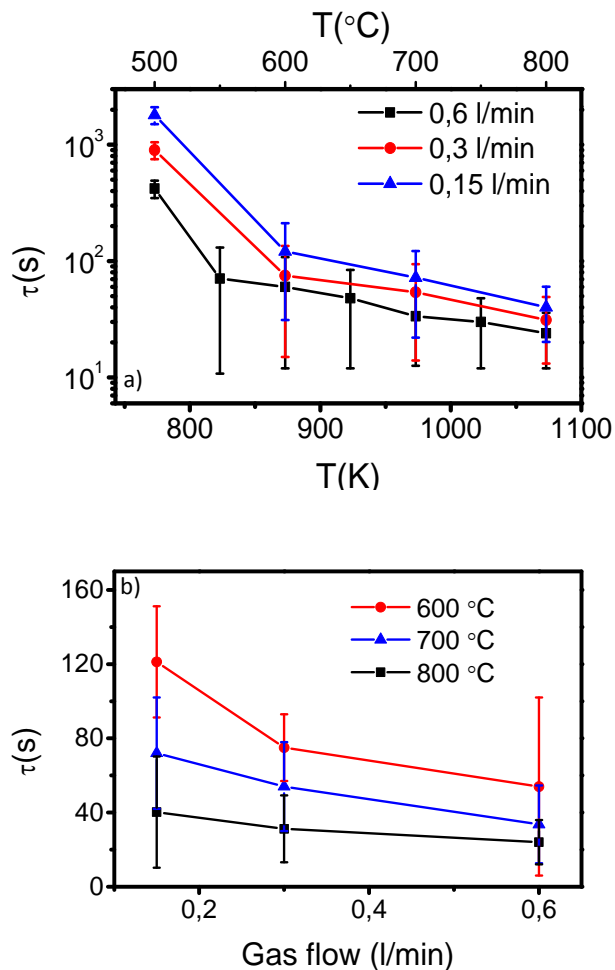


Figure S1. Evolution of the diffusion relaxation time (τ) with a) the temperature for different gas flow values and b) the gas flow for different temperatures.

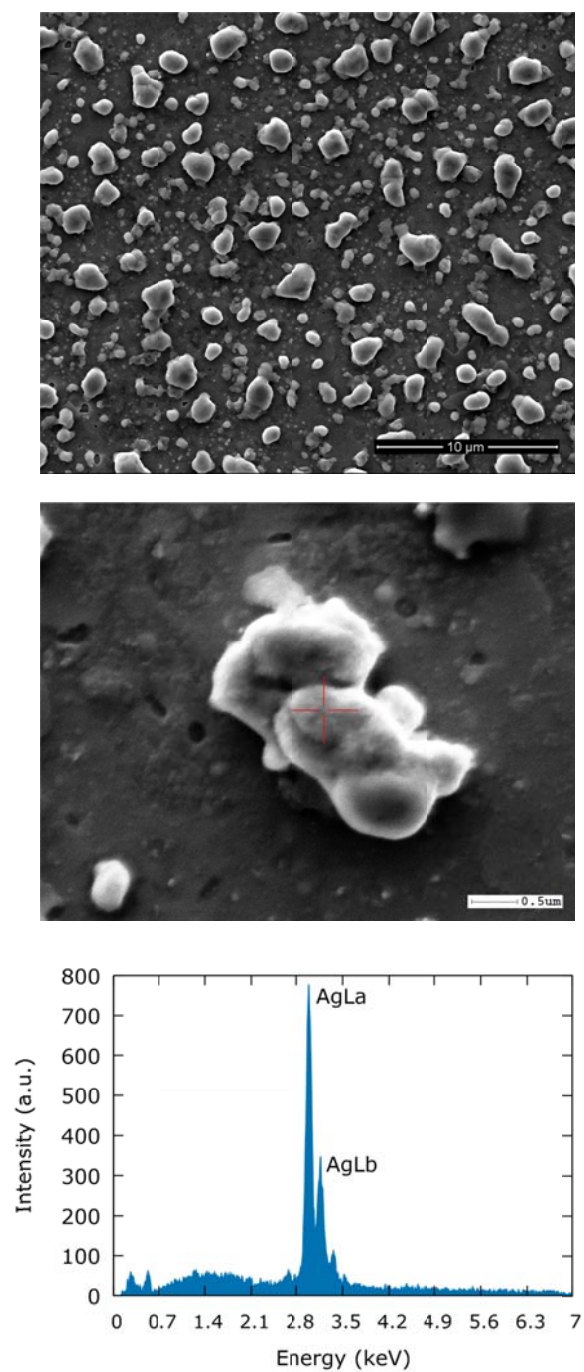


Figure S2. a) SEM image of a YBCO film with a silver coating after annealing at 500 °C. b) Detail of an Ag microparticle where EDX analysis has been carried out. c) EDX analysis of the microparticle observed in b).